GPS+BDS RTK

A Low-Cost Single-Frequency Positioning Approach

BY ROBERT ODOLINSKI AND PETER J.G. TEUNISSEN

GPS has been the number-one positioning tool for a range of applications during the past few decades. The integration of the emerging global navigation satellite systems, such as the Chinese BeiDou Navigation Satellite System (BDS), can give improved precise (millimeter- to centimeter-level) real-time kinematic (RTK) positioning. When BDS is combined with GPS, about double the number of satellites are visible in the Asia-Pacific region, which can make single-frequency RTK and low-cost receiver RTK positioning possible.

In this article, we will analyze the performance of L1 GPS + B1 BDS in Dunedin, New Zealand, using low-cost receivers. We compare their performance to that of L1+L2 GPS survey-grade receivers.

First, we describe the GPS+BDS functional and stochastic models and the data used for our evaluations. Least-squares variance component estimation (LS-VCE) is used as a means to determine the code and phase (co)variances to formulate a realistic stochastic model. (An incorrect stochastic model will deteriorate the ambiguity resolution and consequently the achievable positioning precisions.) Having correctly defined the stochastic model, we focus on the positioning performance. We investigated the ambiguity resolution and positioning performance, both formally and empirically, for customary and high-elevation cut-off angles. The high cut-off angles are used to mimic situations when low-elevation multipath is to be avoided. Lastly, we compared all our results between using low-cost and survey-grade antennas.

GPS+BDS POSITIONING MODEL

The model that we used for positioning is given as follows. Assume that $s_G + 1$ GPS satellites are tracked on f_G frequencies and $s_B + 1$ BDS satellites on f_B frequencies. As we apply system-specific double-differencing (DD), one pivot satellite is used per system. The total number of DD phase and code observations per epoch then equals $2f_G s_G + 2f_B s_B$. We assume for now that cross-correlation between frequencies as well as code and phase is absent. The combined multi-frequency short-baseline GPS+BDS model is then defined as follows.

The system-specific DD phase and code observation vectors are denoted as φ_* and p_*, respectively, with $* = \{G, B\}$ where G = GPS and B = BDS. The single-epoch GNSS model of the combined system is given as

FIGURE 1 Low-cost single-frequency receivers collecting GPS+BDS data for single-baseline RTK, with patch antennas (left) and survey-grade antennas (right) on Jan. 4–6 and Jan. 6–8, 2016, respectively. Survey-grade dual-frequency GPS receivers were connected to the same survey-grade antennas simultaneously to truly track the same GPS constellation.

$$\begin{bmatrix} \varphi \\ p \end{bmatrix} = \begin{bmatrix} \Lambda & A \\ 0 & A \end{bmatrix} \begin{bmatrix} a \\ b \end{bmatrix} + \begin{bmatrix} \varepsilon \\ e \end{bmatrix} \qquad (1)$$

and

$$D \begin{bmatrix} \varphi \\ p \end{bmatrix} = \begin{bmatrix} Q_{\varphi\varphi} & 0 \\ 0 & Q_{pp} \end{bmatrix} \qquad (2)$$

in which

$\varphi = \left[\varphi_G^T, \varphi_B^T \right]^T \in \mathbb{R}^{f_G s_G + f_B s_B}$ is the combined phase vector,

$p = \left[p_G^T, p_B^T \right]^T \in \mathbb{R}^{f_G s_G + f_B s_B}$ is the combined code vector,

$a = \left[a_G^T, a_B^T \right]^T \in \mathbb{Z}^{f_G s_G + f_B s_B}$ is the combined integer ambiguity vector,

$b \in \mathbb{R}^v$ is the real-valued baseline vector,

$\varepsilon = \left[\varepsilon_G^T, \varepsilon_B^T \right]^T \in \mathbb{R}^{f_G s_G + f_B s_B}$ is the combined phase random observation noise vector,

$e = \left[e_G^T, e_B^T \right]^T \in \mathbb{R}^{f_G s_G + f_B s_B}$ is the combined code random observation noise vector, and

$D \left[. \right]$ denotes the dispersion operator.

The entries of the baseline design and wavelength matrices are given as

$$A = \left[A_G^T, A_B^T \right]^T, \quad A_* = \left[\mathbf{e}_{f_*} \otimes \mathbf{D}_{s_*}^T G_* \right]$$

$$\Lambda = \mathrm{blkdiag}\big[\,\Lambda_{\mathrm{G}},\Lambda_{\mathrm{B}}\,\big],\quad \Lambda_* = \mathrm{diag}\big[\,\lambda_{1_*},\ldots,\lambda_{f_*}\,\big]\otimes \mathbf{I}_{s_*}$$

where $\mathbf{e}_{f_*}$ is the $f_*\times 1$ vector of 1s, $\mathbf{D}_{s_*}^{\mathrm{T}}=\big[-\mathbf{e}_{s_*},\mathbf{I}_{s_*}\big]$ is the $s_*\times\big(s_*+1\big)$ differencing matrix, $\mathbf{I}_{s_*}$ is the $s_*\times s_*$ unit matrix, the geometry-matrices $\boldsymbol{G}_G$ and $\boldsymbol{G}_B$ contain the undifferenced receiver-satellite unit direction vectors for GPS and BDS, respectively, λ_{j_*} is the wavelength of frequency j_*, $\otimes$ denotes the Kronecker product, and "diag" and "blkdiag" indicate diagonal and block diagonal matrices, respectively. The entries of the positive definite variance matrices are given as

$$\boldsymbol{Q}_{\varphi\varphi}=\mathrm{blkdiag}\big[\,\boldsymbol{Q}_{\varphi_G\varphi_G},\boldsymbol{Q}_{\varphi_B\varphi_B}\,\big],\boldsymbol{Q}_{\varphi_*\varphi_*}=\boldsymbol{C}_{\varphi_*\varphi_*}\otimes 2\boldsymbol{Q}_*$$

$$\boldsymbol{Q}_{pp}=\mathrm{blkdiag}\big[\,\boldsymbol{Q}_{p_G p_G},\boldsymbol{Q}_{p_B p_B}\,\big],\boldsymbol{Q}_{p_* p_*}=\boldsymbol{C}_{p_* p_*}\otimes 2\boldsymbol{Q}_*$$

$$\boldsymbol{C}_{\varphi_*\varphi_*}=\mathrm{diag}\big[\,\sigma^2_{\varphi_{1_*}},\ldots,\sigma^2_{\varphi_{f_*}}\,\big],\boldsymbol{C}_{p_* p_*}=\mathrm{diag}\big[\,\sigma^2_{p_{1_*}},\ldots,\sigma^2_{p_{f_*}}\,\big] \quad(3)$$

$$\boldsymbol{Q}_*=\mathbf{D}_{s_*}^{\mathrm{T}}\boldsymbol{W}_*^{-1}\mathbf{D}_{s_*},\boldsymbol{W}_*=\mathrm{diag}\big[\,w_{1_*},\ldots,w_{s_*+1}\,\big]$$

where $\sigma_{\varphi_{j_*}},\sigma_{p_{j_*}}$ denote the phase and code standard deviation, respectively, and w_{i_*} the satellite elevation-angle-dependent weight.

The model in Equation 1 applies to short baselines, and thus the ionospheric and tropospheric delays are assumed absent. The broadcast ephemerides are used to obtain the satellite coordinates. Further, the Least-squares AMBiguity Decorrelation Adjustment (LAMBDA) technique is used to estimate the integer ambiguities $\boldsymbol{a}$. The observation noise vectors $\boldsymbol{\varepsilon}$ and $\boldsymbol{e}$, respectively, are zero-mean vectors, provided that no multipath is present in Equation 1.

EXPERIMENT SETUP

The GNSS receivers we used are depicted in **FIGURE 1**. Firstly, two low-cost single-frequency receivers were set up to collect L1+B1 GPS+BDS data for two days. These receivers cost a few hundred U.S. dollars. Since the patch antennas we used have been shown to have less effective signal reception and multipath suppression in comparison to survey-grade antennas, the receivers that collected data for two days were additionally connected to such antennas. These antennas have a cost of slightly more than US$1,000 per antenna. To compare the low-cost solution to a survey-grade receiver-solution, two such receivers (which cost several thousand U.S. dollars) were connected to the same survey-grade

INNOVATION INSIGHTS

BY **RICHARD B. LANGLEY**

ALL GOOD THINGS ARE CHEAP; ALL BAD ARE VERY DEAR. That's what the famous American essayist (and surveyor) Henry David Thoreau wrote in his diary on March 3, 1841. He was likely referring, in part, to the cheapness of the things he came across in nature such as birdsong or the plants and trees on the shores of Walden Pond and the dearness of some luxuries and comforts of civilization, which he tended to eschew. But what has that got to do with GPS, you might ask?

When they were first introduced in the late 1970s and early 1980s, GPS receivers were very dear. Many of them sold for anywhere from $50,000 to $250,000, which would be equivalent to about twice those amounts in today's dollars. The first civilian receivers were large bulky affairs. As I documented in this column in April 1990 ("Smaller and Smaller: The Evolution of the GPS Receiver"), the "first commercially available GPS receiver was the STI-5010 built by Stanford Telecom-

munications Inc. It was a dual-frequency, C/A- and P-code, slow-sequencing receiver. Cycling through four satellites took about five minutes, and the receiver unit alone required about 30 centimeters of rack space. External counters, also requiring rack space, made pseudorange measurements. An external computer controlled the receiver and computed positions." While it could be transported in a small truck (and some were), it was not designed for portability and ease of use by surveyors or geodesists.

Then, in 1982, Texas Instruments introduced the first relatively compact civil GPS receiver, the TI 4100, also known as the Navstar Navigator. And as I also noted in that column more than 15 years ago, this "receiver could make both C/A- and P-code measurements along with carrier-phase measurements on both L1 and L2 frequencies. Its single hardware channel could track four satellites simultaneously through a multiplexing arrangement. The 37 × 45 × 21–centimeter receiver/processor had a

handheld control and display unit and an optional dual–cassette data recorder for saving measurements for postprocessing. The unit, although portable, weighed 25 kilograms and consumed 110 watts of power (the receiver doubled as a hand warmer). Field operation required a supply of automobile batteries."

My, how things have changed. Beginning around 1990, receivers steadily got smaller and smaller and cheaper and cheaper. Survey-grade GNSS (not just GPS) receivers can now be purchased for well under $10,000 and consumer-grade units sell for as little as a hundred dollars or less. And, of course, the GNSS modules inside smartphones and other devices cost manufacturers only a couple of dollars or so. But even a GNSS receiver that can supply raw pseudorange and carrier-phase measurments now costs only a few hundred dollars, and in this month's column, a couple of researchers from Down Under pit a couple of these receivers up against a couple of survey-grade receivers. Did this cheap receiver turn out to be a good thing? Read on to find out.
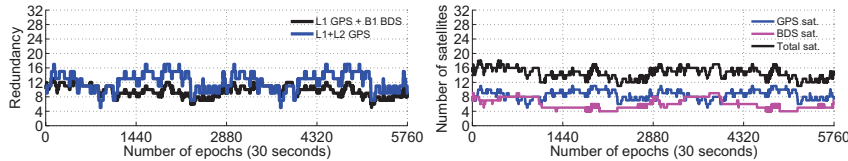
FIGURE 2 Redundancy (left) and number of satellites (right) of L1+B1 GPS+BDS and L1+L2 GPS during Jan. 6–8, 2016, (48 hours) for an elevation cut-off angle of 10°.

antennas through splitters and collected L1+L2 GPS data. A detection, identification and adaption procedure was used to eliminate any outliers.

FIGURE 2 depicts the corresponding redundancy of the two receiver models (that is, the number of observations minus the number of estimated unknowns) together with the number of satellites over 48 hours (30-second epoch interval). The number of BDS satellites (magenta lines) is overall smaller than when compared to GPS (blue lines) in Dunedin. However, Figure 2 also shows that the model strength of L1+B1 GPS+BDS, as measured by its redundancy, is almost similar to that of L1+L2 GPS except for some hours at the middle of the two days. This implies that the two

receiver models can potentially give competitive RTK ambiguity resolution and positioning performance. This is however only true if the receiver code and phase observation noise would be of similar magnitude between the receivers used, hence the need for an analysis of the receiver observation precision.

In our receiver evaluations, we determined a set of reference ambiguities by using a known baseline and treating them as time-constant parameters over the two days in a dynamic model.

LOW-COST RTK POSITIONING
The code and phase variances were estimated by LS-VCE using data independent from the data used for

the following positioning analysis. The variances are needed to formulate a realistic stochastic model, whereas an incorrect stochastic model will deteriorate the ambiguity resolution and consequently the achievable positioning precisions. **TABLE 1** depicts the corresponding estimated standard deviations (STDs) used for our positioning models.

Table 1 shows that the code precision of L1 GPS and B1 BDS improves significantly when the survey-grade antennas are used instead of patch antennas (49 centimeters STD for L1/B1 that decreases to about 30 centimeters), due to their better signal reception and multipath suppression abilities. For testing our stochastic model, we used data that is independent from the data used to estimate the code/phase precision.

Positioning Performance. The single-epoch (instantaneous) RTK positioning results for 24 hours data are shown in **FIGURE 3**, with ambiguity-float solutions shown at the top and ambiguity-fixed solutions at the
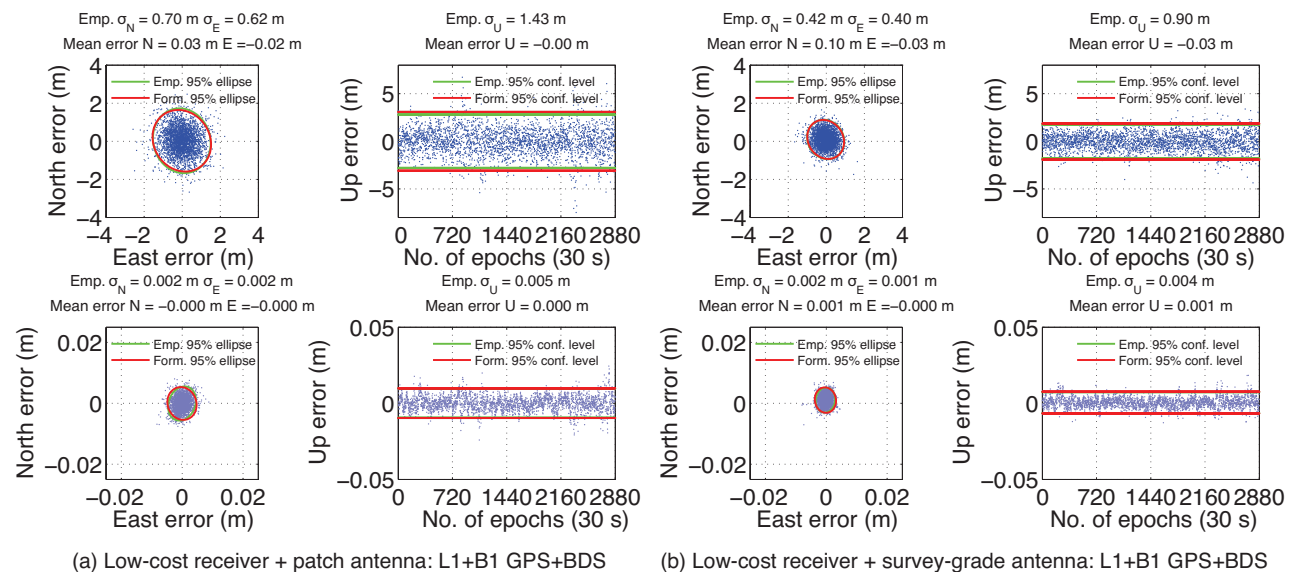

Emp. σ_N = 0.70 m σ_E = 0.62 m
Mean error N = 0.03 m E = −0.02 m

Emp. σ_U = 1.43 m
Mean error U = −0.00 m

Emp. σ_N = 0.42 m σ_E = 0.40 m
Mean error N = 0.10 m E = −0.03 m

Emp. σ_U = 0.90 m
Mean error U = −0.03 m

Emp. σ_N = 0.002 m σ_E = 0.002 m
Mean error N = −0.000 m E = −0.000 m

Emp. σ_U = 0.005 m
Mean error U = 0.000 m

Emp. σ_N = 0.002 m σ_E = 0.001 m
Mean error N = 0.001 m E = −0.000 m

Emp. σ_U = 0.004 m
Mean error U = 0.001 m

(a) Low-cost receiver + patch antenna: L1+B1 GPS+BDS   (b) Low-cost receiver + survey-grade antenna: L1+B1 GPS+BDS

FIGURE 3 Horizontal (north (N), east (E)) position scatter and corresponding vertical (U) time series of the float (top) and *correctly* fixed (bottom) L1+B1 GPS+BDS single-epoch RTK solutions for an elevation cut-off angle of 10°. The 95% empirical and formal confidence ellipses and intervals are shown in green and red, respectively. The 24 hour (30 second) period is 22:00-22:00 UTC Jan. 5-6, 2016, for patch antennas in (a) and 21:48-21:48 UTC Jan. 8-9, 2016, for survey-grade antennas in (b), which are periods independent of the periods used to determine the stochastic model through the code/phase STDs in Table 1.

Receiver/ antenna	System	Frequency	STD code (cm)	STD phase (mm)
Survey-grade/ survey-grade	GPS	L1 L2	18 20	2 2
Low-cost/ survey-grade	GPS BDS	L1 B1	31 30	2 2
Low-cost/patch	GPS BDS	L1 B1	49 49	2 2

TABLE 1 Zenith-referenced undifferenced code and phase standard deviations estimated by least-squares variance component estimation.

bottom. Only the correctly fixed solutions are depicted as determined by comparing the instantaneously estimated ambiguities to the set of reference ambiguities. The 95% empirical and formal confidence ellipses and intervals are shown in green and red, respectively. They were computed from the empirical and formal position variance matrices. The empirical variance matrix was estimated from the positioning errors as obtained from comparing the estimated positions to precise benchmark coordinates. The formal variance matrix used was determined from the mean of all single-epoch formal variance matrices.

Figure 3 shows a good fit between the formal and empirical confidence ellipses/intervals, which thus illustrates realistic LS-VCE STDs in Table 1 that were used in the stochastic model. Note also the two-order of magnitude improvement when going from float to fixed solutions, and that the low-cost receiver plus survey-grade antenna has the most precise ambiguity-float positioning solutions.

Ambiguity Resolution and Positioning Performance for Higher Cut-Off Angles. We subsequently investigated the low-cost L1+B1 GPS+BDS performance for high elevation cut-off angles, so as to mimic situations in urban canyon environments or when low-elevation-angle multipath is present and is to be avoided. We have made comparisons to the survey-grade L1+L2 GPS results. It has been shown that a good ambiguity resolution performance does not necessarily imply a good positioning performance, so we investigated what effect this has on our positioning models.
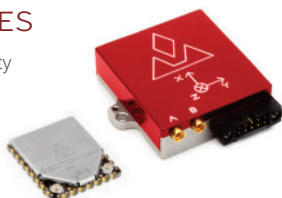
The following integer least-squares (ILS) success rates (SRs) are thus computed based on epochs with the condition of positional dilution of precision (PDOP) ≤ 10 and averaged over all epochs over two days of data. By including and excluding epochs with large PDOPs, we can show how the positioning performance of the different models is affected by poor receiver-satellite geometries. To better understand how this exclusion of epochs with large PDOPs also influenced the empirical ambiguity-correctly-fixed positioning performance, we constructed **TABLE 2**, which shows the corresponding positioning STDs for two
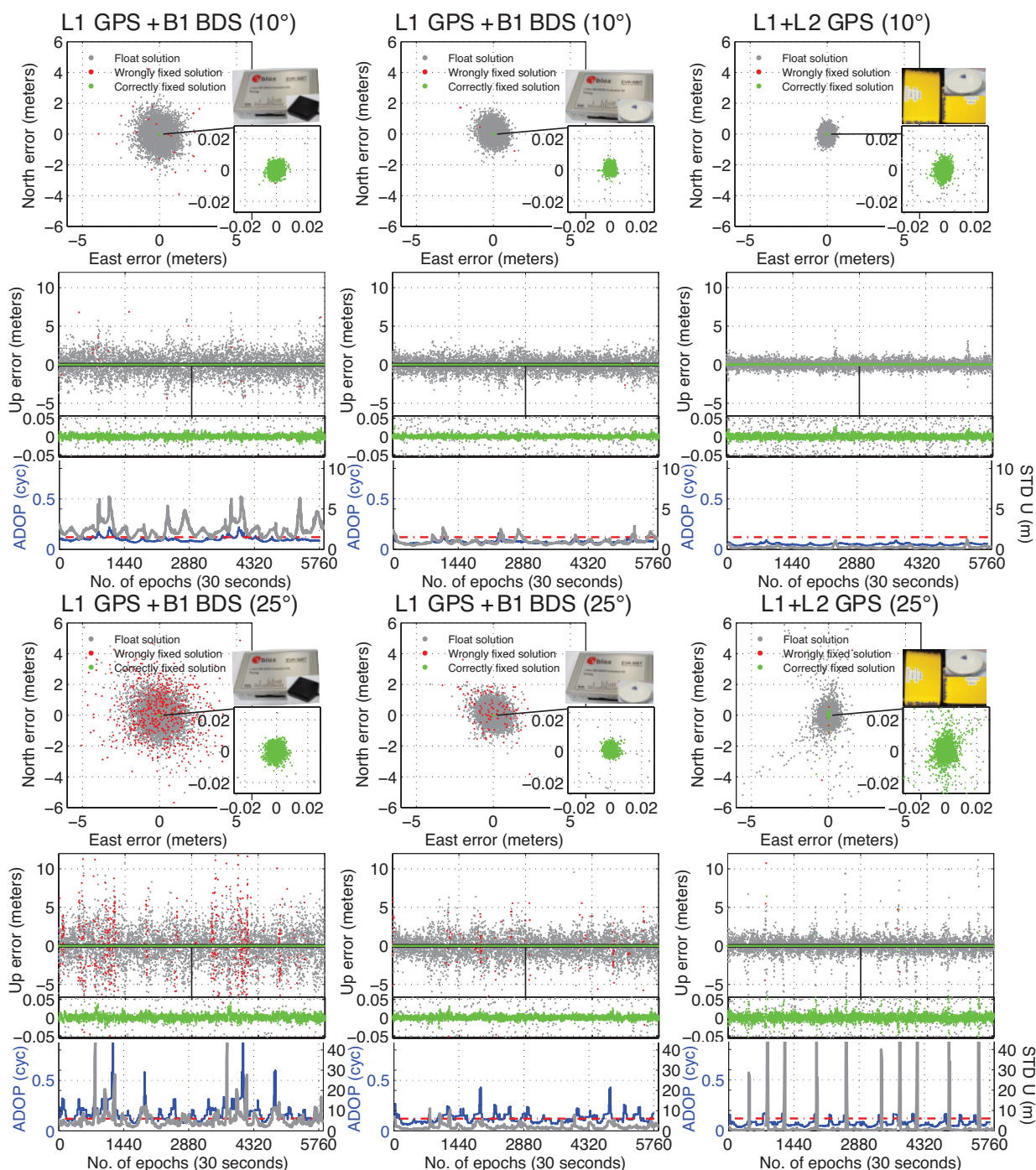
FIGURE 4 Horizontal (N, E) scatterplots and vertical (U) time series for L1+B1 low-cost receiver with patch antenna (first column) with 99.5% (89.8%) ILS SR, L1+B1 low-cost receiver with survey-grade antenna (second column) with 100% (97.8%) ILS SR, and survey-grade L1+L2 GPS (third column) with 100% (94.1%) ILS SR, using 10º (top two rows) and 25º (bottom two rows) cut-off angles respectively (Jan. 4–6, 2016, for low-cost receiver with patch antenna and Jan. 7–8, 2016, for the low-cost and survey-grade receivers with survey-grade antennas). The SRs are conditioned on PDOP ≤ 10 and computed based on all epochs. Below the vertical time series, the ADOP is depicted in blue color, the 0.12-cycles level as red, and ambiguity-float vertical formal STDs are shown in gray.

Positioning model	Empirical STDs (mm), ILS SR (%)															
Cut-off (°):	20				25				30				35			
	N	E	U	SR	N	E	U	SR	N	E	U	SR	N	E	U	SR
L1+L2 survey-grade	3	2	7	99.9	90	23	114	99.4	73	27	195	93.0	75	37	229	80.2
PDOP ≤ 10	3	2	6	99.5	3	3	8	94.1	4	3	9	81.8	5	3	11	64.1
L1+B1 low-cost receiver and survey-grade antenna	2	1	4	99.8	2	2	5	97.8	2	2	6	77.3	2	2	7	50.3
PDOP ≤ 10									2	2	6	76.7	2	2	6	48.8
L1+B1 low-cost receiver and patch antenna	2	2	6	96.9	3	2	7	89.8	3	2	8	57.3	3	4	12	25.0
PDOP ≤ 10									3	2	8	57.0	3	3	10	24.9

TABLE 2 Single-epoch empirical STDs (N, E, U) of *correctly* fixed positions for the three positioning models together with their ILS SR for four elevation cut-off angles and 48 hours of data (Jan. 4–6 and Jan. 6–8, 2016). The empirical STDs and ILS SRs are also shown when conditioned on PDOP ≤ 10.

days of data. These STDs were computed by comparing the estimated positions to precise benchmark coordinates. In addition to the positioning performance, we depict in Table 2 the corresponding empirical ILS SR for full ambiguity-resolution, which is given by the ratio of the number of correctly fixed epochs to the total number of epochs.

Table 2 shows that the L1+B1 low-cost receiver plus patch antenna combination has (as expected) smaller SRs in comparison to those when the survey-grade antenna is used. This latter combination has comparable SRs to the (PDOP-conditioned) SRs of the survey-grade L1+L2 GPS receiver for cut-off angles up to 25°.

In support of better understanding Table 2, **FIGURE 4** shows typical positioning results for the different receiver and antenna combinations with elevation cut-off angles of 10° (top two rows) and 25° (bottom two rows). The first and third rows show the local horizontal (N, E) positioning scatterplots and the second and fourth rows the vertical (U) time series over two days of data. The float solutions are depicted in gray, and incorrectly and correctly fixed solutions in red and green, respectively. The zoom-in is given to better show the spread of the correctly fixed solutions with millimeter-centimeter level precisions. The formal ambiguity-float STDs are also shown under the up time series to reflect consistency between the empirical and formal positioning results.

We also depict in Figure 4 the ambiguity dilution of precision (ADOP) as an easy-to-compute scalar diagnostic to measure the intrinsic model strength for successful ambiguity resolution. The ADOP is defined as

$$\text{ADOP} = \sqrt{\left|\boldsymbol{Q}_{\hat{a}\hat{a}}\right|^{\frac{1}{n}}} \text{ (cycles)} \qquad (4)$$

with n being the dimension of the ambiguity vector, $\boldsymbol{Q}_{\hat{a}\hat{a}}$ the ambiguity variance matrix, and $|.|$ denoting the determinant. ADOP gives a good approximation to the average precision of the ambiguities, and it also provides for a good approximation to the ILS SR. The rule-of-thumb is

that an ADOP smaller than about 0.12 cycles corresponds to an ambiguity SR larger than 99.9%.

Figure 4 shows that more solutions are incorrectly fixed (red dots) when the ADOPs (blue lines) are larger than the 0.12 cycle level (red dashed lines). The figure also reveals that the L1+B1 low-cost receiver plus patch antenna combination achieves an ILS SR (99.5%) similar to that of the survey-grade L1+L2 GPS receiver (SR of 100%) for the cut-off angle of 10°. This ILS SR corresponds to the availability of correctly fixed solutions (green dots) with millimeter-centimeter level positioning precision over the

two days. The L1+L2 GPS receiver has, moreover, large ambiguity-fixed positioning excursions at the same time as the formal STDs are large for the cut-off angle of 25° due the poor GPS-only receiver-satellite geometry for this high cut-off angle. This is also reflected by the corresponding relatively large ambiguity-fixed STDs depicted in Table 2 that are improved from decimeter- to millimeter-level when the PDOP ≤ 10 condition is applied. Figure 4 also shows that the L1+B1 low-cost receiver with the survey-grade antenna has a larger SR of 97.8% when compared to the PDOP-conditioned SR for L1+L2 GPS of 94.1% for the cut-off angle of 25° (see also Table 2), owing to the use of BDS that significantly improves the receiver-satellite geometry.

Finally, we also tested the low-cost receiver-solution (with survey-grade antennas) for a baseline length of 7 kilometers, where (small) residual slant ionospheric delays are present. It was shown that this combination still has the potential to achieve ambiguity resolution and positioning performance competitive with the survey-grade receiver-solution.

CONCLUSIONS

In this article, we evaluated a low-cost L1+B1 GPS+BDS RTK setup and compared its ambiguity resolution and positioning performance to a survey-grade L1+L2 GPS solution in Dunedin, New Zealand. The LS-VCE procedure was used to determine the variances of the low-cost receivers. The estimated variances are needed so as to formulate a realistic stochastic model, otherwise the ambiguity resolution and hence the achievable positioning precisions would deteriorate.

Since we analyzed a short baseline, the LS-VCE variances were shown to likely be affected by multipath. To mitigate multipath we connected the low-cost receivers to survey-grade antennas with better signal reception and multipath suppression abilities. It was shown that the survey-grade antennas can significantly improve the performance for the low-cost receivers so that the code/phase noise estimates more resemble that of survey-grade receivers. The LS-VCE STDs were furthermore shown to be realistically estimated for an independent time period.

We also demonstrated that the low-cost receivers can give competitive instantaneous ambiguity resolution and positioning performance to that of the survey-grade receivers. This is particularly true when the low-cost receivers are connected to survey-grade antennas.

MANUFACTURERS

The low-cost receivers used in the research were u-blox (*www.u-blox.com*) EVK-M8T receivers. The survey-grade receivers were Trimble (*www.trimble.com*) NetRS receivers. The patch antennas were u-blox ANN-MS antennas, while the survey-grade antennas were Trimble Zephyr 2 GNSS antennas. ◉

ROBERT ODOLINSKI conducted his Ph.D. studies at Curtin University, Perth, Australia, from 2011 to 2014. His research focus is next-generation multi-GNSS integer ambiguity resolution enabled precise positioning. In 2015, Odolinski started his position as a lecturer/research fellow in geodesy/GNSS at the School of Surveying, University of Otago, New Zealand.

PETER J.G. TEUNISSEN is a professor of geodesy and navigation and the head of the Curtin GNSS Research Centre, Curtin University. He is also with the Department of Geoscience and Remote Sensing, Delft University of Technology, Delft, The Netherlands. His research interests include multiple GNSS and the modeling of next-generation GNSS for high-precision positioning, navigation and timing applications.